High Resolution Energy-Angle Correlation Measurement of Hard X Rays from Laser-Thomson Backscattering

A. Jochmann,[1,2,*] A. Irman,[1] M. Bussmann,[1] J. P. Couperus,[1,2] T. E. Cowan,[1,2] A. D. Debus,[1] M. Kuntzsch,[1,2] K. W. D. Ledingham,[3] U. Lehnert,[1] R. Sauerbrey,[1,2] H. P. Schlenvoigt,[1] D. Seipt,[1,4] Th. Stöhlker,[4,5] D. B. Thorn,[5] S. Trotsenko,[4,5] A. Wagner,[1] and U. Schramm[1,2]

[1]*Institute of Radiation Physics, Helmholtz-Zentrum Dresden - Rossendorf, Bautzner Landstrasse 400, 01328 Dresden, Germany*
[2]*Technische Universität Dresden, 01062 Dresden, Germany*
[3]*SUPA, Strathclyde University Glasgow, UK-07743 Glasgow, United Kingdom*
[4]*Helmholtz-Institut Jena, Friedrich Schiller Universität Jena, 07743 Jena, Germany*
[5]*GSI Helmholtzzentrum für Schwerionenforschung GmbH, 64291 Darmstadt, Germany*

(Received 6 May 2013; published 13 September 2013)

Thomson backscattering of intense laser pulses from relativistic electrons not only allows for the generation of bright x-ray pulses but also for the investigation of the complex particle dynamics at the interaction point. For this purpose a complete spectral characterization of a Thomson source powered by a compact linear electron accelerator is performed with unprecedented angular and energy resolution. A rigorous statistical analysis comparing experimental data to 3D simulations enables, e.g., the extraction of the angular distribution of electrons with 1.5% accuracy and, in total, provides predictive capability for the future high brightness hard x-ray source PHOENIX (photon electron collider for narrow bandwidth intense x rays) and potential gamma-ray sources.

DOI: 10.1103/PhysRevLett.111.114803 PACS numbers: 41.50.+h, 34.80.Qb, 41.75.Fr, 52.59.Px

Ultrashort, nearly monochromatic hard x-ray pulses generated at 4th generation light sources [1] enrich the understanding of the ultrafast dynamics of atomic lattice structures [2,3]. However more complex and/or destructive processes such as in high-energy-density physics [4,5], high pressure physics [6], and ultra-high-intensity laser matter interactions [7] require single shot experiments, in which the full spectroscopic or structural dataset must be obtained in a single exposure. For this type of experiment, which is inherently less reproducible, a finite-bandwidth x-ray pulse (up to a few percent) is desirable to cover the spectral region of interest in one exposure. In strong field science there is a growing interest in fundamental processes between strong laser fields and relativistic electrons, e.g., radiation reaction [8], pair creation [9], and vacuum birefringence [10]. Pushed by such demands, advanced x-ray sources based on scattering of an ultrashort laser pulse off a relativistic electron beam (also called relativistic Thomson scattering or inverse Compton scattering [11,12]) are becoming important. Besides providing intense pulses with finite bandwidth, tunable from hard x rays [13–18] to the γ-ray range [19–21], Thomson scattering can also serve as a laboratory for strong field physics and nonlinear interactions [22].

The focus of this Letter lies on the detailed understanding of the kinematics during the interaction in the linear regime. Hence, we performed a full characterization of the emitted spectrum to reveal parameter influences and correlations of both interacting beams, performed an *ab initio* comparison with the 3D radiation code CLARA [23], and validated an analytical scaling relation for the mean x-ray energy on axis. In this regime, the pulsed laser field can be interpreted as an optical undulator with spatially and temporally varying field strength. Oscillating electrons emit Doppler-upshifted radiation into a relativistically contracted solid angle cone in the laboratory frame. For one relativistic electron ($v \approx c$) oscillating in a linearly polarized laser field (ω_0) the angular frequency of the scattered photon ω_{sc} scales as [24]

$$\omega_{sc} = \frac{2\gamma^2(1-\cos\varphi)}{1+(a_0^2/2)+\gamma^2\theta^2}\,\omega_0, \tag{1}$$

where φ is the collision angle ($\varphi = 180°$ for a head-on geometry). The dimensionless laser strength parameter a_0 ($= 0.85 \times 10^{-9}\lambda[\mu\mathrm{m}](I[\mathrm{W/cm^2}])^{1/2}$) is negligible in the linear regime. The emission or observation angle θ is measured with respect to the average electron propagation direction (beam axis) and $\gamma = 1/\sqrt{1-(v^2/c^2)}$ is the Lorentz factor. The maximum photon energy $E_{max} = 4\gamma^2 E_0$ is detected along the axis for a head-on geometry. Any deviation in either collision or observation angle from a head-on geometry reduces the Doppler shift, resulting in lower photon energies.

A finite bandwidth of a Thomson scattering x-ray source is the result from the complex interplay between electron energy spread ($\Delta\gamma$), electron beam emittance ($\propto \Delta\varphi$), laser focusing geometry ($\Delta\vec{k} \propto \Delta\varphi$), laser bandwidth ($\Delta\omega_0$), and detector solid angle ($\Delta\Omega_{Det}$) [23]. An ensemble of electrons in a bunch crosses the interaction plane at multiple angles relative to the beam axis due to the beam transverse emittance as sketched in Fig. 1(a). The electron

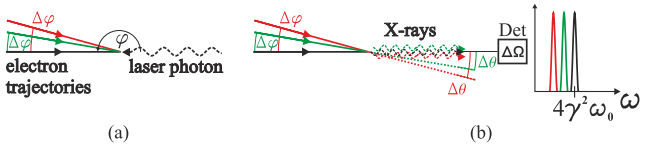

FIG. 1 (color online). Schematic of the interaction for a head-on geometry ($\varphi = \pi$) including kinematic effects ($\Delta\varphi$) (a) as well as detector size ($\Delta\Omega_{\mathrm{Det}}$). The detector is placed on the electron beam axis ($\theta = 0$) (b).

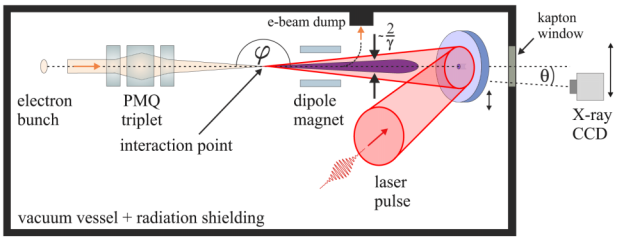

FIG. 2 (color online). Experimental setup of the Thomson backscattering source at the ELBE accelerator.

direction deviation $\Delta\varphi$ has to be added to the observation angle and therefore causes an observation angle spread $\Delta\theta$ [see Fig. 1(b)]. Due to superposition of the emitted x-ray photons, the detected x-ray spectrum is broadened. For a detector placed at $\theta = 0$ these photons can only contribute to the low-energy tail of the spectral distribution ($\omega < 4\gamma^2\omega_0$). This effect caused by the θ dependence in Eq. (1) results in a skewed x-ray spectrum assuming symmetric distributions of the electron beam energy and the laser bandwidth. In this case, the x-ray bandwidth ($\Delta\omega/\omega$) scales with the laser bandwidth ($\sim \Delta\omega_0/\omega_0$), the electron energy spread ($\sim 2\Delta\gamma/\gamma$), and the electron beam emittance ($\sim \gamma^2\Delta\varphi^2$). Due to the finite size of the detector, it collects scattered x-ray photons emitted in a certain solid angle, also increasing the detected x-ray bandwidth ($\sim \gamma^2\Delta\Omega_{\mathrm{Det}}^2$) [19,25].

In previous experiments the spectral characteristics of Thomson scattering were deduced from indirect filter-pack measurements [17,21,26,27] or with single element semiconductor detection systems [13–16]. Both methods suffer from limited detector resolution and a low signal-to-noise ratio. In this Letter we report the influence of the electron beam emittance, the laser bandwidth, and the energy-angle correlation on the bandwidth of the scattered x rays. We suppress the influence of laser focusing by using a long focal length parabola ($f/30$) which makes the interaction length [23] longer than each beam's pulse length. The spectra were collected by a pixelated detector (CCD camera) at various observation angles and analyzed by a single photon counting technique [28,29]. In order to minimize additional spectral broadening caused by the detector size, we analyzed datasets from small clusters of pixels. To our knowledge this is the first complete spectral characterization of a Thomson scattering source with high angular and high energy resolution.

The experiment was carried out at HZDR with the DRACO Ti:sapphire laser system [30] and the ELBE linear accelerator facility [31] and based on the head-on collision ($\varphi = 180°$) schematically shown in Fig. 2. The front end of this laser system delivered pulse energies of 100 mJ centered at 800 nm with a bandwidth of about 20 nm (rms) on target in a nearly diffraction limited spot (35 μm FWHM). This resulted in $a_0 = 0.05$. The laser covered a photon energy range from 1.49 to 1.61 eV. The ELBE accelerator provided electron bunches of 22.5 MeV kinetic energy with a 0.25% energy spread and a 4 ps (FWHM) duration [32]. The bunch charge was 77 pC. The electron beam was focused to the laser focal plane to an elliptical spot with major and minor axis $a = 136$ μm (rms) and $b = 103$ μm (rms). The projections onto the x and y axis are $\sigma_X = 124$ μm and $\sigma_Y = 115$ μm. The focal spot ratio of both beams ensured constant spatial overlap during the experiment. The normalized transverse emittance of the beam was (16 ± 2) mm mrad measured in front of the last focusing element, a permanent magnet quadrupole (PMQ) triplet. The laser system was actively synchronized to the accelerator with a time jitter better than 1 ps [32]. The x-ray photons were collected in a 1024×256 pixel back-illuminated CCD camera (ANDOR DY420-BR-DD), mounted on a translation stage for the y direction. The camera was calibrated for photon counting spectroscopy using radioactive sources (^{241}Am and ^{55}Fe) taking into account the intrinsic detector response including quantum efficiency as well as any transmitted material (vacuum windows, air, filter material). In our measurements the energy bin width was 30 eV and the linewidth resolution was 100 eV (rms). The incident photon energy was calculated from the charge deposited in one pixel. An x-ray spectrum was obtained by counting single-pixel-absorption events (SPAE) from a 50×50 pixel area on the CCD chip. This size corresponds to an angular resolution of 0.6 mrad which guaranteed the detection of the intrinsic bandwidth inhibiting any broadening effects due to the finite detector size [15]. For the camera used the SPAE algorithm is limited to a photon flux on the order of 1×10^5 photons/cm^2, defining the closest detector position.

To quantitatively predict and analyze the scattering process, the radiation code CLARA [23] has been used, which is based on solving the Liénard-Wiechert potentials. The simulation takes realistic experimental parameters as input. This includes the full focusing geometry of the laser and electron beam, the laser spectral shape, the ponderomotive force, the space charge effect, as well as the collection solid angle. Additionally the electron beam transverse and longitudinal emittances are implemented. In contrast to summing scattering probabilities over the electron and photon phase space using standard Monte Carlo techniques, this code also takes into account

the phase of the emitted radiation. The latter is important in the nonlinear Thomson scattering regime, which will be the topic of future experiments.

Simulation results have been compared to experimental data by analyzing x-ray peak energy, spectral shape, and amplitude at all observation angles for various electron beam angular spreads (σ_φ) for a fixed spot size. The optimal simulated parameter set was obtained using maximum likelihood methods [33].

Figure 3(a) shows recorded x-ray spectra (blue curves) at increasing observation angles (θ from 0 to 18 mrad in the y-z plane) in the plane perpendicular to the laser polarization. One trace was built by integrating 900 shots at one fixed observation angle. The simulated angle-dependent spectra are presented as a color code distribution underlying the experimental data. It is clearly visible that the measured x-ray spectrum shifts to lower photon energies for larger emission angles. The trend follows the prediction from the simulation. Also plotted (black dotted line) is the analytical result from Eq. (1). The measured maximum cutoff energy is about 13.1 keV which agrees well with Eq. (1) taking a laser energy of 1.61 eV and an electron energy of 22.5 MeV. The spectrum peaks at 12.3 keV on the axis ($\theta = 0$) and shifts to 8.2 keV at $\theta = 18.0$ mrad. The positions of the x-ray peaks are found to deviate from Eq. (1), particularly near the electron beam propagation axis. This is an effect due to the angular spread of the incoming electrons, which destroys the simple correlation between the scattered photon energy and the observation direction in Eq. (1). Figure 3(b) shows two spectra at observation angles $\theta = 1.15$ and 11.6 mrad. The spectrum near the electron beam axis has a narrower bandwidth and is skewed with a pronounced tail to lower x-ray energies. The spectrum at $\theta = 11.6$ mrad is symmetric whereas the bandwidth has approximately doubled and the amplitude has dropped by a factor of 2. For a quantitative measure of the shape, we performed an accurate analysis of the statistical moments of the x-ray spectra.

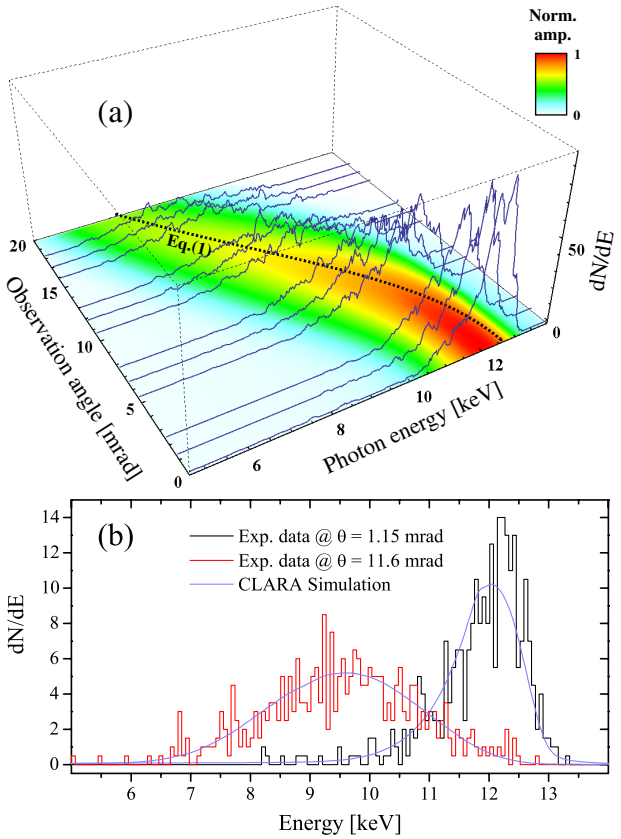

FIG. 3 (color online). Full data set (QE corrected) combined with CLARA simulation results and Eq. (1) (dotted black line) (a) and exemplary raw data spectra at observation angles $\theta = 1.15$ and 11.6 mrad to illustrate changes in the shape of the distribution (b).

Figures 4(a)–4(c) display the x-ray energy (1st moment: mean μ), the x-ray spectral bandwidth (2nd moment: standard deviation σ), and asymmetry [quantified by 3rd moment: skewness $= (1/\sum c_i)\sum c_i(x_i - \mu)^3/\sigma^3$ with c_i being the counts at bin x_i] from the experimental data for different emission angles (black dots). The simulated quantities (narrow black line) show good agreement within a 1σ-confidence interval (shaded area). Figure 4(a) illustrates that for laminar beams (angular spread $\sigma_\varphi = 0$) the energy-angle correlation is consistent with Eq. (1). However, for an electron beam with $\sigma_\varphi > 0$, the x-ray mean energy near the axis is redshifted. On axis it can be estimated by averaging ω_{sc} over a distribution $f(\varphi)$ of collision angles φ, using a monochromatic plane wave approximation. The integral $\langle\omega_{sc}\rangle = \int d\varphi f(\varphi)\omega_{sc}(\varphi)$ can be solved by expanding ω_{sc} in powers of the angle φ with $\Delta\varphi = \sigma_\varphi = \epsilon_n/(\gamma\sigma_r)$ leading to

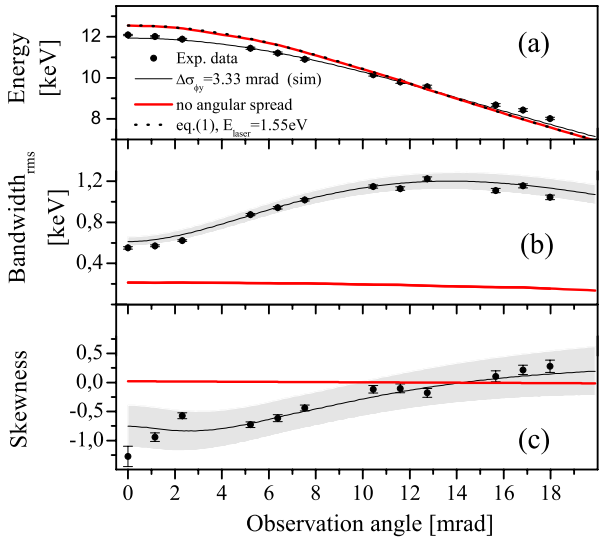

FIG. 4 (color online). Analysis of the statistical moments, mean μ, standard deviation σ, and skewness. The shaded area represents a 1σ-confidence interval from the CLARA simulation. The horizontal uncertainty is 0.6 mrad.

$$\langle \omega_{sc} \rangle_{\theta=0} \approx 4\gamma^2 \omega_0 (1 - 2(\gamma \Delta\varphi)^2). \quad (2)$$

The difference of $\langle \omega_{sc} \rangle$ from Eq. (2) and CLARA is about 1% which is below the detector resolution.

In Fig. 4(b) the narrowest bandwidth is found in the electron beam forward direction ($\theta = 0$ mrad). At this position a bandwidth of 0.55 keV (rms) was obtained which corresponds to a relative bandwidth of $\Delta\omega_{sc}/\omega_{sc,peak} \approx$ 4.5% (rms). The energy spread of the electron beam ($\Delta\gamma/\gamma \approx 0.1\%$) is sufficiently small, so its contribution to the bandwidth is negligible. Thus the main contribution to the bandwidth originates from the electron beam angular spread [3.34 mrad (rms)] and the laser bandwidth [$\Delta\lambda/\lambda \approx$ 2.5% (rms)]. As the observation angle increases, the bandwidth becomes larger reaching the broadest bandwidth for $\theta > 10$ mrad. In Fig. 4(b) the simulated case for a laminar electron beam ($\sigma_{\varphi y} = 0$) is plotted for comparison (thick red line). In this case the spectral bandwidth is narrower and approximately constant at all observation angles for sufficiently small collection angles ($\Delta\Omega_{Det} < 1$ mrad). The influence of the electron beam emittance can also be seen in the symmetry of the x-ray spectrum as shown in Fig. 4(c). Close to the beam forward direction the spectrum shows strong asymmetry as a long tail to the low-energy side. With increasing observation angle the spectral distribution becomes more symmetric. The skewness changes sign at $\theta \approx 14$ mrad and asymptotically approaches zero for larger observation angles. The behavior for angles $\theta > 20$ mrad has been extracted from CLARA simulations. Simulation and experimental data are consistent for the θ range accessible in the experiment. Also plotted is the simulated skewness for a laminar electron beam [thick red line in Fig. 4(c)]. For this case the spectral shape is symmetric and independent of the emission angle.

The sensitivity for the spectral shape and bandwidth can be used to deduce the electron beam angular spread by comparing simulation results with experimental data. The quality of the data, being almost background free, and the high angular resolution allow us to use the entire data set (350 histogram bins at 12 detector positions) in a maximum likelihood fit. Minimizing the Poisson likelihood chi square [33] using simulations of various angular distributions, assuming a fixed spot size, an electron beam angular spread of (3.34 ± 0.05) mrad has been determined. With the free parameters angular spread and flux, the reduced χ^2 is 0.77. At the focus the electron beam transverse emittance is correlated to the angular spread via $\epsilon_n = \beta\gamma\sigma_\varphi\sigma_r$. With the measured quantities $\gamma = 45 \pm 0.25\%$, $\sigma_{\varphi y} = (3.34 \pm 0.05)$ mrad and $\sigma_Y = (115 \pm 6)$ μm the deduced normalized emittance is $\epsilon_{ny} = (17.48 \pm 1.22)$ mm mrad. The result agrees with the machine parameters; the uncertainty is dominated by the spot size measurement.

For single-shot x-ray experiments the number of photons per shot is crucial. In the current setup with a 1.2 pC interacting charge due to the spatial overlap, we detected 13 photons per shot on axis in a solid angle of 0.36π μsr. Utilizing the full capacity of the DRACO laser system and the ELBE superconducting photogun [34], laser pulses with energies above 1 J and interacting bunch charges up to 1 nC are feasible. Using these parameters, maintaining a laser intensity for the linear regime, we estimate an x-ray yield of 1×10^8 photons per shot within 1.6π msr($\sim 1/\gamma$) or 1×10^5 photons per shot with $\Delta\omega/\omega = 4.5\%$ (rms) in a solid angle of 0.36π μsr (corresponding to a 600 μm x-ray spot 1 m away from the interaction point). This will make PHOENIX a competitive x-ray source with a finite bandwidth well suited for many types of time-resolved measurements in the subpicosecond regime. It will become an important development platform for more demanding experiments at the future European XFEL facility. In the future the brightness of laser-Thomson light sources can be further increased by employing the novel traveling wave Thomson scattering scheme [35].

In conclusion, we showed that high resolution angle and energy resolved data can be used to determine the individual influence of beam parameters on the x-ray photon distribution with high sensitivity. We developed a simple scaling law to predict the mean energy on the beam axis for angular spreads σ_φ smaller than 4 mrad. The angular distribution of electrons has a strong influence on the Thomson x-ray spectral shape and bandwidth. Controlling this spread (the ratio of beam emittance and spot size) is necessary for designing Thomson x-ray sources with a specific bandwidth suited to an application. As a next step, the understanding of the interaction in the linear regime needs to be extended to the nonlinear regime for testing existing scaling laws [23,36] and high field QED effects to quantify the distinction from classical Thomson scattering [37].

The authors thank the teams from ELBE and DRACO as well as B. Kämpfer, J. Metzkes, R. Pausch, W. Seidel, W. Wagner, and K. Zeil for their support and fruitful discussions. This work was supported by EC FP7 LASERLAB-EUROPE/CHARPAC (Contract No. 284464).

*a.jochmann@hzdr.de

[1] Y. Ding *et al.*, Phys. Rev. Lett. **109**, 254802 (2012).
[2] S. M. Vinko *et al.*, Nature (London) **482**, 59 (2012).
[3] H. N. Chapman *et al.*, Nature (London) **470**, 73 (2011).
[4] P. Patel, A. Mackinnon, M. Key, T. Cowan, M. Foord, M. Allen, D. Price, H. Ruhl, P. Springer, and R. Stephens, Phys. Rev. Lett. **91**, 125004 (2003).
[5] F. Perez *et al.*, Phys. Rev. Lett. **104**, 085001 (2010).
[6] H.-P. Liermann, W. Morgenroth, A. Ehnes, A. Berghäuser, B. Winkler, H. Franz, and E. Weckert, J. Phys. Conf. Ser. **215**, 012029 (2010).
[7] Y. Sentoku, E. d'Humières, L. Romagnani, P. Audebert, and J. Fuchs, Phys. Rev. Lett. **107**, 135005 (2011).
[8] C. Harvey, T. Heinzl, and M. Marklund, Phys. Rev. D **84**, 116005 (2011).

[9] E. Lötstedt, U. Jentschura, and C. Keitel, Phys. Rev. Lett. **101**, 203001 (2008).
[10] T. Heinzl, B. Liesfeld, K.-U. Amthor, H. Schwoerer, R. Sauerbrey, and A. Wipf, Opt. Commun. **267**, 318 (2006).
[11] R. Milburn, Phys. Rev. Lett. **10**, 75 (1963).
[12] E. Esarey, S. Ride, and P. Sprangle, Phys. Rev. E **48**, 3003 (1993).
[13] R. W. Schoenlein, W. P. Leemans, A. H. Chin, P. Volfbeyn, T. E. Glover, P. Balling, M. Zolotorev, K.-J. Kim, S. Chattopadhyay, and C. V. Shank, Science **274**, 236 (1996).
[14] W. Leemans, R. Schoenlein, P. Volfbeyn, A. Chin, T. Glover, P. Balling, M. Zolotorev, K. Kim, S. Chattopadhyay, and C. Shank, Phys. Rev. Lett. **77**, 4182 (1996).
[15] K. Chouffani, F. Harmon, D. Wells, J. Jones, and G. Lancaster, Phys. Rev. ST Accel. Beams **9**, 050701 (2006).
[16] A. Jochmann *et al.*, Nucl. Instrum. Methods Phys. Res., Sect. B **309**, 214 (2013).
[17] I. V. Pogorelsky *et al.*, Phys. Rev. ST Accel. Beams **3**, 090702 (2000).
[18] G. Priebe *et al.*, Proc. SPIE Int. Soc. Opt. Eng. **7805**, 780513 (2010).
[19] F. Albert, S. G. Anderson, D. J. Gibson, R. A. Marsh, S. S. Wu, C. W. Siders, C. P. J. Barty, and F. V. Hartemann, Phys. Rev. ST Accel. Beams **14**, 050703 (2011).
[20] N. Pietralla *et al.*, Phys. Rev. Lett. **88**, 012502 (2001).
[21] S. Chen *et al.*, Phys. Rev. Lett. **110**, 155003 (2013).
[22] D. Seipt and B. Kämpfer, Phys. Rev. A **83**, 022101 (2011).
[23] A. Debus *et al.*, Proc. SPIE Int. Soc. Opt. Eng. **7359**, 735908 (2009).
[24] S. K. Ride, E. Esarey, and M. Baine, Phys. Rev. E **52**, 5425 (1995).
[25] F. Hartemann, H. Baldis, A. Kerman, A. Le Foll, N. Luhmann, and B. Rupp, Phys. Rev. E **64**, 016501 (2001).
[26] D. J. Gibson *et al.*, Phys. Rev. ST Accel. Beams **13**, 070703 (2010).
[27] K. Ta Phuoc, S. Corde, C. Thaury, V. Malka, A. Tafzi, J. P. Goddet, R. C. Shah, S. Sebban, and A. Rousse, Nat. Photonics **6**, 308 (2012).
[28] D. B. Thorn *et al.*, Rev. Sci. Instrum. **81**, 10E325 (2010).
[29] G. Plateau *et al.*, Phys. Rev. Lett. **109**, 064802 (2012).
[30] K. Zeil, S. D. Kraft, S. Bock, M. Bussmann, T. E. Cowan, T. Kluge, J. Metzkes, T. Richter, R. Sauerbrey, and U. Schramm, New J. Phys. **12**, 045015 (2010).
[31] F. Gabriel, P. Gippner, E. Grosse, D. Janssen, P. Michel, H. Prade, A. Schamlott, W. Seidel, A. Wolf, and R. Wünsch, Nucl. Instrum. Methods Phys. Res., Sect. B **161–163**, 1143 (2000).
[32] C. Kaya *et al.*, Appl. Phys. Lett. **100**, 141103 (2012).
[33] S. Baker and R. Cousins, Nucl. Instrum. Methods Phys. Res., Sect. B **221**, 437 (1984).
[34] J. Teichert *et al.*, J. Phys. Conf. Ser. **298**, 012008 (2011).
[35] A. Debus, M. Bussmann, M. Siebold, A. Jochmann, U. Schramm, T. E. Cowan, and R. Sauerbrey, Appl. Phys. B **100**, 61 (2010).
[36] D. Seipt and B. Kämpfer, Phys. Rev. ST Accel. Beams **14**, 040704 (2011).
[37] T. Heinzl, D. Seipt, and B. Kämpfer, Phys. Rev. A **81**, 022125 (2010).
[38] See Supplemental Material at http://link.aps.org/supplemental/10.1103/PhysRevLett.111.114803 for [brief description].